Eur. J. Mech. B - Fluids 19 (2000) 229–252

S0997-7546(00)00109-6/FLA

Small Reynolds number instabilities in two-layer Couette flow

Fabrice Albert, François Charru *

Institut de Mécanique des Fluides de Toulouse, UMR CNRS/INPT-UPS 5502, 2 allée du Professeur Camille Soula, 31400 Toulouse, France

(Received 12 July 1999; revised 21 December 1999; accepted 23 December 1999)

Abstract – Instabilities in two-layer Couette flow are investigated from a small Reynolds number expansion of the eigenvalue problem governing linear stability. The wave velocity and growth rate are given explicitly, and previous results for long waves and short waves are retrieved as special cases. In addition to the inertial instability due to viscous stratification, the flow may be subject to the Rayleigh–Taylor instability. As a result of the competition of these two instabilities, inertia may completely stabilise a gravity-unstable flow above some finite critical Froude number, or conversely, for a gravity-stable flow, inertia may give rise to finite wavenumber instability above some finite critical Weber number. General conditions for these phenomena are given, as well as exact or approximate values of the critical numbers. The validity domain of the many asymptotic expansions is then investigated from comparison with the numerical solution. It appears that the small-Re expansion gives good results beyond $\mathrm{Re} = 1$, with an error less that 1%. For Reynolds numbers of a few hundred, we show from the eigenfunctions and the energy equation that the nature of the instability changes: instability still arises from the interfacial mode (there is no mode crossing), but this mode takes all the features of a shear mode. The other modes correspond to the stable eigenmodes of the single-layer Couette flow, which are recovered when one fluid is rigidified by increasing its viscosity or surface tension.

hydrodynamic instability / interfacial waves

1. Introduction

The flow of two or more superposed viscous fluid layers driven by gravity or pressure gradient is encountered in many industrial processes, such as coating or polymer extrusion. A striking feature of this kind of flow is that it may be destabilised by any inertial effect, whatever small, due to an interfacial mode of instability. This feature has been first pointed out by Yih [1], who showed that Couette and Poiseuille two-layer flows may be unstable to long wavelength disturbances, with a growth rate proportional to $\alpha_1^2\,\mathrm{Re}$, where $\alpha_1 := kh_1$ is the dimensionless wavenumber and $\mathrm{Re} := a_1 h_1^2/\nu_1$ is the Reynolds number (see *figure 1* for definitions). Instability typically arises when the thinner layer is the more viscous, a phenomenon known as the 'thin layer effect' [2]. Short wave instability was investigated by Hooper and Boyd [3], who showed that Couette flow may be unstable when surface tension effects are negligible, with a growth rate proportional to Re/α_1^2; for fluids with same density, this instability occurs for any viscosity ratio. The mechanism of the short wave instability has been described by Hinch [4], whereas an explanation of the 'thin layer effect' has been proposed by Charru and Hinch [5].

The long and short wave expansions of Yih, and Hooper and Boyd do not give the stability against intermediate wavenumbers, $\alpha_1 = \mathrm{O}(1)$. This domain has been studied by Hooper [6], by an expansion in powers of the small parameter $\beta^{-3} = \mathrm{Re}/\alpha_1^2$, where β is the viscous penetration depth of interfacial disturbances, assumed to be large compared to the wavelength. However, this study is restricted to equal densities, and

* Correspondence and reprints; e-mail: charru@imft.fr

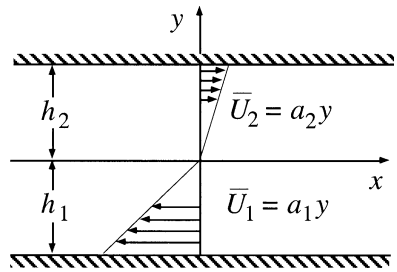

Figure 1. Two-layer Couette flow.

appears to be merely a correction of the short wave expansion for $\alpha_1 = O(1)$, which does not give the right wave velocity and growth rate of long waves. In addition to asymptotic studies, numerical studies have been performed [6–9], showing that for some parameter values, instability may occur for finite Reynolds number with finite wavenumber.

Experimental evidence of the long wave and short wave instabilities has been given for Couette flow in closed channel by several studies [10–12]. These studies also show that instability leads to finite amplitude interfacial waves, as predicted by nonlinear analyses [13–17].

For higher Reynolds numbers, numerical studies as well as matched asymptotic expansions [7] reveal that multi-layer flows may be unstable to shear waves, characterised by eigenfunctions with their maximum near the walls, for critical Reynolds number of order 1000 and finite critical wavenumber of order 1. Experimental evidence of this shear mode of instability has been given by Kao and Park [18] (see also Yiantsos and Higgins [9]). An other important related situation, first studied by Miles [19], is that of a thin viscous fluid sheared by a bulk flow, typically gas flow over a liquid film [20]. This flow may exhibit boundary layer instability as well as interfacial instability, which may interact [21,22].

Thus, much is known about interfacial instabilities in two-layer flows. However, a global outlook is still lacking, partly due to the number of different scales that have been used; the validity domains of the various asymptotic studies as well as their possible overlap have not been clarified, and the degree of generality of some numerical results remains unclear. The aim of this paper is to propose a unified view of small Reynolds number instabilities in two-layer Couette flow, from a small-Re expansion of the linear stability problem. Such a shear driven flow may appear of less practical relevance than pressure or gravity driven flows. However, the main ingredient of small Reynolds number instabilities is the slope discontinuity of the velocity profile due to the viscosity difference and two-layer Couette flow is the simplest flow that exhibits this discontinuity (as an exception, vertical core-annular flow may be unstable due to density difference [23]). Thus, the main features of the unified view we propose hold for more general shear flows. Moreover, as pointed out by Pozrikidis [24], the study of viscous interfacial shear flows may contribute to our understanding of heterogeneous mixing due to mechanical agitation.

The governing equations are given in Section 2. Section 3 is devoted to the small-Re results, for Froude number $Fr \ll 1$, $Fr \gg 1$ and $Fr = O(1)$, successively. The main previous results are retrieved as special cases. The case $Fr = O(1)$ corresponds to competing Rayleigh–Taylor and inertial instabilities, which may result, for finite Re and for a wide range of flow parameters, in one of the two noticeable cases: (i) complete restabilisation of the Rayleigh–Taylor instability by inertia, and (ii) onset of inertial instability with finite critical wavenumber. The validity domain of the small-Re expansion, as well as that of the long and short wave expansions, is investigated in Section 4 by solving numerically the eigenvalue problem. In Section 5, the nature of the instability is discussed from inspection of the eigenfunctions and the energy equation, along with an incursion in the domain of higher Reynolds numbers.

2. The linearised problem

In order to cover both the long wave and short wave behaviours, we take the inverse wavenumber k^{-1} as the unit length, and then assume transverse gradients to be of order unity. The unit time is taken as the inverse shear rate a_1^{-1}; and the unit pressure, as $\mu_1 a_1$. Dimensional quantities, if necessary, will be noted with the superscript 'dim'. We define for each fluid a dimensionless thickness:

$$\alpha_j := kh_j, \quad j = 1, 2. \tag{1}$$

Then, we define the viscosity ratio m, the thickness ratio d and the density ratio r:

$$M := \frac{\mu_2}{\mu_1}, \qquad r := \frac{\rho_2}{\rho_1}, \qquad d := \frac{h_2}{h_1}, \tag{2}$$

and the Reynolds number, the Weber number and the Froude number:

$$\mathrm{Re} := \frac{a_1 h_1^2}{\nu_1}, \qquad \mathrm{We} := \frac{\rho_1 a_1^2 h_1^3}{\gamma}, \qquad \mathrm{Fr} := \frac{a_1^2 h_1}{(1-r)g}, \tag{3a}$$

which measure the effects of inertia against those of viscosity, surface tension γ and gravity g, respectively. The parameter d is not independent since $\alpha_2 = d\alpha_1$, and for fixed d, the thickness α_1 can alternatively be considered as the wavenumber of the disturbance. For future use we also define the capillary number, the Bond number and the Galileo number:

$$\mathrm{Ca} := \frac{\mathrm{We}}{\mathrm{Re}} = \frac{\mu_1 a_1 h_1}{\gamma}, \qquad \mathrm{Bo} := \frac{\mathrm{We}}{\mathrm{Fr}} = \frac{(\rho_1 - \rho_2) g h_1^2}{\gamma}, \qquad \mathrm{Ga} := \frac{\mathrm{Re}^2}{\mathrm{Fr}} = \frac{(1-r)\rho_1^2 g h_1^3}{\mu_1^2}. \tag{3b}$$

Note that the last two do not depend on the shear rate.

Although the problem can be solved using streamfunctions, we keep velocities and pressure as unknowns. The velocity $\mathbf{u}_j = (U_j, V_j)$ and pressure P_j are considered as the superposition of a basic-state flow, corresponding to a flat interface ($\overline{\eta} = 0$), and small disturbances:

$$U_j = \overline{U}_j + u_j, \qquad V_j = \overline{V}_j + v_j, \qquad P_j = \overline{P}_j + p_j,$$

where the basic-state flow is given by:

$$\overline{U}_1 = y, \qquad \overline{U}_2 = y/m, \qquad \overline{V}_1 = \overline{V}_2 = 0, \qquad \overline{\eta} = 0, \tag{4a}$$

$$\overline{P}_1(y) - P_0 = -\frac{\mathrm{Re}}{\alpha_1(1-r)\mathrm{Fr}} y, \qquad \overline{P}_2(y) - P_0 = -\frac{r\mathrm{Re}}{\alpha_1(1-r)\mathrm{Fr}} y, \tag{4b}$$

where P_0 is a reference pressure at the interface. Looking for small amplitude disturbances ($k\eta \ll 1$) as normal modes:

$$(u_j, v_j, p_j, \eta) = \frac{1}{2}\big((\hat{u}_j(y), \hat{v}_j(y), \hat{p}_j(y), \hat{\eta})\mathrm{e}^{i(x-ct)} + \text{c.c.}\big),$$

where c.c. denotes complex conjugate, the linearised mass and momentum conservation equations give, for the amplitude of the disturbances:

$$i\hat{u}_j + \partial_y \hat{v}_j = 0, \quad j = 1, 2, \tag{5a}$$

$$\frac{r_j \mathrm{Re}}{\alpha_1^2}\big(i(y/m_j - c)\hat{u}_j + \hat{v}_j/m_j\big) = -i\hat{p}_j + m_j\big(-\hat{u}_j + \partial_{yy}\hat{u}_j\big), \quad j = 1, 2, \tag{5b}$$

$$i\frac{r_j \mathrm{Re}}{\alpha_1^2}(y/m_j - c)\hat{v}_j = -\partial_y \hat{p}_j + m_j\big(-\hat{v}_j + \partial_{yy}\hat{v}_j\big), \quad j = 1, 2, \tag{5c}$$

where $r_1 = 1$, $r_2 = r$, $m_1 = 1$, $m_2 = m$. The no-slip conditions at the walls are:

$$\hat{u}_1(-\alpha_1) = 0, \qquad \hat{v}_1(-\alpha_1) = 0, \tag{6a}$$

$$\hat{u}_2(\alpha_2) = 0, \qquad \hat{v}_2(\alpha_2) = 0. \tag{6b}$$

The linearised equations at the interface $y = 0$ for continuity of each component of velocity and stress are respectively:

$$\hat{\eta} + \hat{u}_1 = \frac{\hat{\eta}}{m} + \hat{u}_2, \tag{7a}$$

$$\hat{v}_1 = \hat{v}_2, \tag{7b}$$

$$\partial_y \hat{u}_1 + i\hat{v}_1 = m\big(\partial_y \hat{u}_2 + i\hat{v}_2\big), \tag{7c}$$

$$-\big(\hat{p}_2 - \hat{p}_1\big) + 2m\partial_y \hat{v}_2 - 2\partial_y \hat{v}_1 = \mathrm{Re}\left(\frac{1}{\mathrm{Fr}} + \frac{\alpha_1^2}{\mathrm{We}}\right)\frac{\hat{\eta}}{\alpha_1} \tag{7d}$$

(note that $\hat{\eta}/\alpha_1 = \hat{\eta}^{\mathrm{dim}}/h_1$ remains finite as α_1 tends to zero or infinity). Finally, the linearised no-mass transfer (or kinematic condition) at the interface is:

$$i\hat{\eta}c + \hat{v}_j = 0. \tag{8}$$

3. Small Reynolds number expansion

In order to solve equations (5)–(8), we choose the normalisation condition $\hat{\eta} = 1$ for the amplitude of the eigenfunctions, and perform a small-Re expansion of these amplitudes and of the eigenvalue c, similar to that performed by Yih [25] for liquid films falling on an inclined plane:

$$\hat{u}_j = \hat{u}_j^{(0)} + \mathrm{Re}\,\hat{u}_j^{(1)} + \cdots,$$

$$\hat{v}_j = \hat{v}_j^{(0)} + \mathrm{Re}\,\hat{v}_j^{(1)} + \cdots,$$

$$\hat{p}_j = \hat{p}_j^{(0)} + \mathrm{Re}\,\hat{p}_j^{(1)} + \cdots,$$

$$c = c^{(0)} + \mathrm{Re}\,c^{(1)} + \cdots. \tag{9}$$

3.1. Strong gravity and surface tension effects: $\mathrm{We} \ll 1$, $\mathrm{Fr} \ll 1$

We first consider the case of strong gravity and surface tension effects, i.e. $\mathrm{We} \ll 1$ and $\mathrm{Fr} \ll 1$, or more precisely $\mathrm{Ca} = \mathrm{O}(1)$ and $\mathrm{Bo} = \mathrm{O}(1)$. The derivation from (5)–(8) of the zeroth-order conservation equations and boundary conditions is straightforward. The hypothesis $\mathrm{Ca} = \mathrm{O}(1)$ leads to keep the gravity and surface tension effects in the normal stress equation at the interface (7d).

The general solution, satisfying the conservation equations and the no-slip conditions at the walls, is found in terms of the hyperbolic sine and cosine functions sh and ch:

$$\begin{aligned} i\hat{v}_j^{(0)} &= (A_j Y_j - B_j)\mathrm{sh}\, Y_j + B_j Y_j \mathrm{ch}\, Y_j, \\ \hat{u}_j^{(0)} &= i\partial_y \hat{v}_j^{(0)} = (B_j Y_j + A_j)\mathrm{sh}\, Y_j + A_j Y_j \mathrm{ch}\, Y_j, \quad j = 1, 2, \\ i\hat{p}_j^{(0)} &= 2m_j\alpha_1^2(A_j \mathrm{sh}\, Y_j + B_j \mathrm{ch}\, Y_j), \end{aligned} \tag{10}$$

where $Y_1 := y + \alpha_1$ and $Y_2 := y - \alpha_2$. The constants A_j and B_j are determined from the four interfacial conditions, which can be written under matrix form $MX_0 = b_0$, where M, b_0 and the solution $X_0 := (A_1, B_1, A_2, B_2)$ are given in Appendix 1. The kinematic condition (8) then gives the eigenvalue $c^{(0)} = c_0 + i\sigma_0$, where c_0 and σ_0 are respectively the wave velocity and growth rate of the normal mode:

$$\frac{c^{\mathrm{dim}}}{a_1 h_1} = \frac{c_0}{\alpha_1} = \frac{1-m}{\alpha_1 D}\big(\alpha_1^2(\mathrm{sh}\, 2\alpha_2 - 2\alpha_2) + \alpha_2^2(\mathrm{sh}\, 2\alpha_1 - 2\alpha_1)\big), \tag{11}$$

$$\frac{\sigma^{\mathrm{dim}}}{a_1} = \sigma_0 = -\frac{\mathrm{Bo} + \alpha_1^2}{2\mathrm{Ca}\,\alpha_1 D}\big((\mathrm{sh}\, 2\alpha_1 - 2\alpha_1)\big(\mathrm{sh}^2\alpha_2 - \alpha_2^2\big) + m(\mathrm{sh}\, 2\alpha_2 - 2\alpha_2)\big(\mathrm{sh}^2\alpha_1 - \alpha_1^2\big)\big), \tag{12}$$

with

$$D = 2m^2\big(\mathrm{sh}^2\alpha_1 - \alpha_1^2\big)\big(\mathrm{ch}^2\alpha_2 + \alpha_2^2\big) + 2\big(\mathrm{ch}^2\alpha_1 + \alpha_1^2\big)\big(\mathrm{sh}^2\alpha_2 - \alpha_2^2\big) + m\big(\mathrm{sh}\, 2\alpha_1\, \mathrm{sh}\, 2\alpha_2 + 4\alpha_1^2\alpha_2^2 - 4\alpha_1\alpha_2\big).$$

The creeping flow wave velocity (11) only depends on the viscosity ratio and thickness of the layers, and it satisfies the symmetry relation:

$$c_0(\alpha_1, \alpha_2, m) = -\frac{1}{m} c_0\left(\alpha_2, \alpha_1, \frac{1}{m}\right).$$

The sign of c_0 is that of $(1-m)$, so that waves propagate in the direction of the less viscous fluid motion. For $m < 1$, the wave velocity is positive and, as shown in *figure 2*, it decreases monotonously to zero, except for high d for which it first increases before decreasing to zero. *Figure 2* also displays previous asymptotic results for long and short waves. The long wave limit of (11) ($\alpha_1 \to 0$, fixed $d = h_2/h_1$) is given by:

$$\frac{c^{\mathrm{dim}}}{a_1 h_1} = \frac{c_0}{\alpha_1} \sim \frac{2(1-m)d^2(1+d)}{(d^2-m)^2 + 4md(1+d)^2}, \quad \alpha_1 \to 0. \tag{13}$$

It exactly corresponds to Yih's long wave result [1]. The short wave limit of (11) ($\alpha_1 \to \infty$, fixed d) is:

$$c_0 \sim \frac{4(1-m)}{(1+m)^2}\alpha_1^2\big(\exp(-2\alpha_1) + d^2\exp(-2d\alpha_1)\big), \quad \alpha_1 \to \infty. \tag{14}$$

This limit predicts an exponential decay with wavenumber. In their short wave expansion in powers of Re/α_1^2, Hooper and Boyd [3] found $c_0 = 0$ at the dominant order ($\mathrm{Re}/\alpha_1^2 = 0$). This creeping flow result differs from

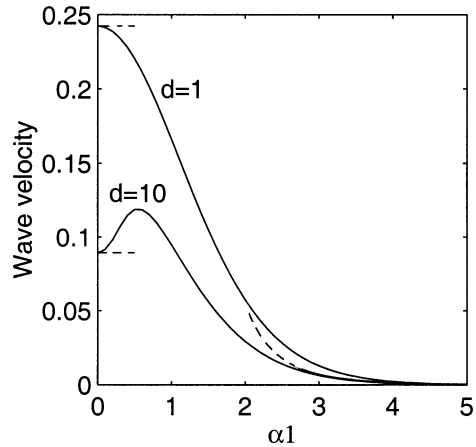

Figure 2. Wave velocity (11) for $d = 1$ and $d = 10$ (plain curves), and long wave (13) and short wave (15) results (dashed curves). $m = 0.5$.

(14) by exponentially small terms only, this difference corresponding to the fact that taking the limit $\alpha_1 \to \infty$ after the limit $\mathrm{Re} \to 0$ is not equivalent to taking the limit $\mathrm{Re}/\alpha_1^2 \to 0$. At the order $(\mathrm{Re}/\alpha_1^2)^2$ Hooper and Boyd found:

$$c_0 = \left(\frac{\mathrm{Re}}{\alpha_1^2}\right)^2 \frac{(1-m)}{16m^4(1+m)^2}\left(5m^4 + 12m^3 - 20m^2 + 12m + 5\right), \quad \frac{\mathrm{Re}}{\alpha_1^2} = \frac{\rho_1 a_1}{\mu_1 k^2} \to 0. \tag{15}$$

This inertial correction (inertial effects are of order Re/α_1^2) predicts algebraic decay. The present small-Re expansion would probably recover this decay at order Re^2. However, *figure 2* shows that for high wavenumbers the absolute difference between (11) and (15) remains small.

A more comprehensive picture of the dependence of the wave velocity on viscosity and thickness ratios can be found in *figure 3*, which displays isovalues in the (m, d) plane for four values of the wavenumber, $\alpha_1 = 0.1, 1, 3$ and 10. These plots show that the wave velocity no longer depends on d as soon as $d > 6/\alpha_1$, i.e. for $\alpha_2 > 6$, which means that a wall does not play any role as soon as the wavelength is smaller than the thickness of the fluid layer.

The creeping flow growth rate (12) corresponds to that of the viscous Rayleigh–Taylor instability of the interface between two fluid layers of finite thickness. Indeed, it depends crucially on gravity and surface tension (all waves are neutral for zero gravity and surface tension), and the dimensional growth rate $a_1\sigma_0$ does not depend on the shear rate a_1. Its sign is that of $-(\mathrm{Bo} + \alpha_1^2)$: it is positive for long waves when the Bond number Bo is negative ($\rho_2 > \rho_1$) due to the destabilising effect of gravity, and it is negative otherwise (*figure 4*). When $\rho_2 > \rho_1$, the cut-off wavenumber $\alpha_{1c} = (-\mathrm{Bo})^{1/2}$, i.e. $k_c = ((\rho_2 - \rho_1)g/\gamma)^{1/2}$, does not depend on viscosity and layer thickness, and is equal to that of the inviscid case [26].

Figure 4 also shows the asymptotic curves for long and short waves. In the long wave limit ($\alpha_1 \to 0$, fixed d), the growth rate is:

$$\sigma_0 \sim -\alpha_1^2 \frac{\mathrm{Bo}}{\mathrm{Ca}} S(m, d), \quad \alpha_1 \to 0, \tag{16}$$

with

$$S(m, d) = \frac{d^3(m + d)}{3(d^4 + 4dm + 6d^2m + 4d^3m + m^2)},$$

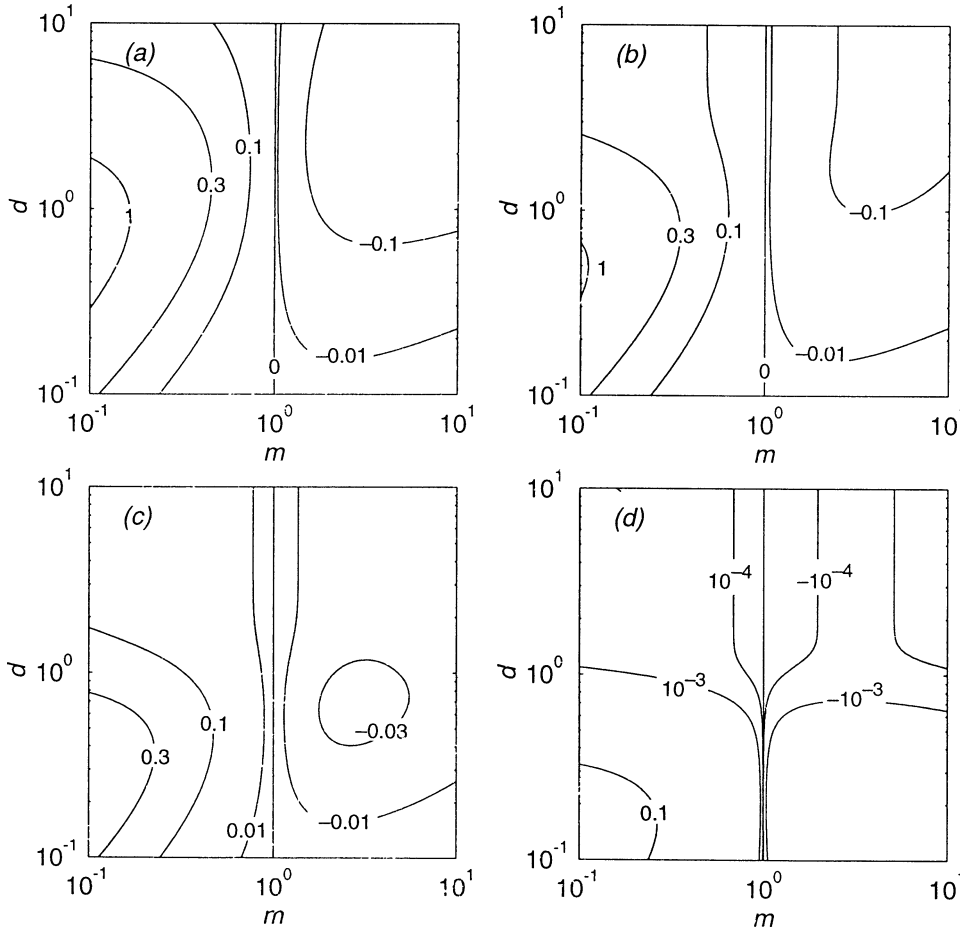

Figure 3. Isovalues of the wave velocity (11) in the (m, d) plane. (a) $\alpha_1 = 0.1$; (b) $\alpha_1 = 1$; (c) $\alpha_1 = 2$; (d) $\alpha_1 = 5$.

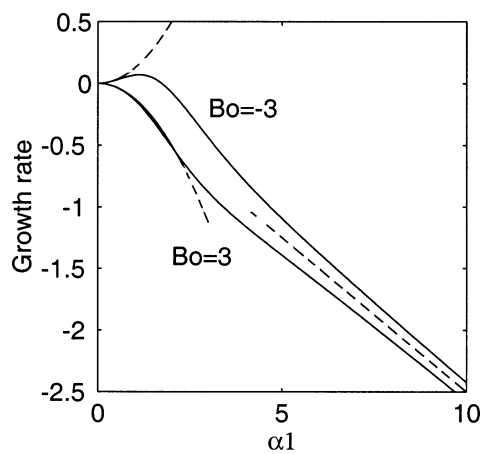

Figure 4. Growth rate (12) for $\mathrm{Bo} = -3$ and $\mathrm{Bo} = 3$ (plain curves), and long wave (16) and short wave (17) results (dashed curves). $m = 1$, $d = 1$, $\mathrm{Ca} = 1$.

corresponding to dimensional growth rate $a_1\sigma_0 \sim -(\rho_1-\rho_2)gh_1^3k^2/\mu_1$. In the short wave limit ($\alpha_1 \to \infty$, fixed d), the growth rate is:

$$\sigma_0 \sim -\frac{\alpha_1}{2\mathrm{Ca}(1+m)}, \quad \alpha_1 \to \infty, \tag{17}$$

corresponding to dimensional growth rate $a_1\sigma_0 \sim -k\gamma/(\mu_1+\mu_2)$. Taking the semi-bounded flow limit ($d=\infty$) gives the result of Yiantsos and Higgins [27], equation (4) for creeping flow, which shows that although the derivation of (12) assumes $d = \mathrm{O}(1)$, it gives the correct result for $d=\infty$.

Figure 5 displays isovalues of the growth rate (12) in the (m,d) plane, for four values of the wavenumber, $\alpha_1 = 0.1, 0.9, 3$ and 10. Cases (a) and (b) correspond to unstable wavenumbers ($\alpha_1 < \alpha_{1c} = 1$), and cases (c) and (d) correspond to stable wavenumbers ($\alpha_1 > \alpha_{1c} = 1$). It appears that the growth rate no longer depends on d for $d > 3/\alpha_1$, i.e. for $\alpha_2 > 3$, which means that a wall does not play any role as soon as the wavelength is less than twice the thickness of the fluid layer. Finally, note that the case of equal viscosities ($m=1$) plays no particular role for the growth rate, unlike its effect on the wave velocity.

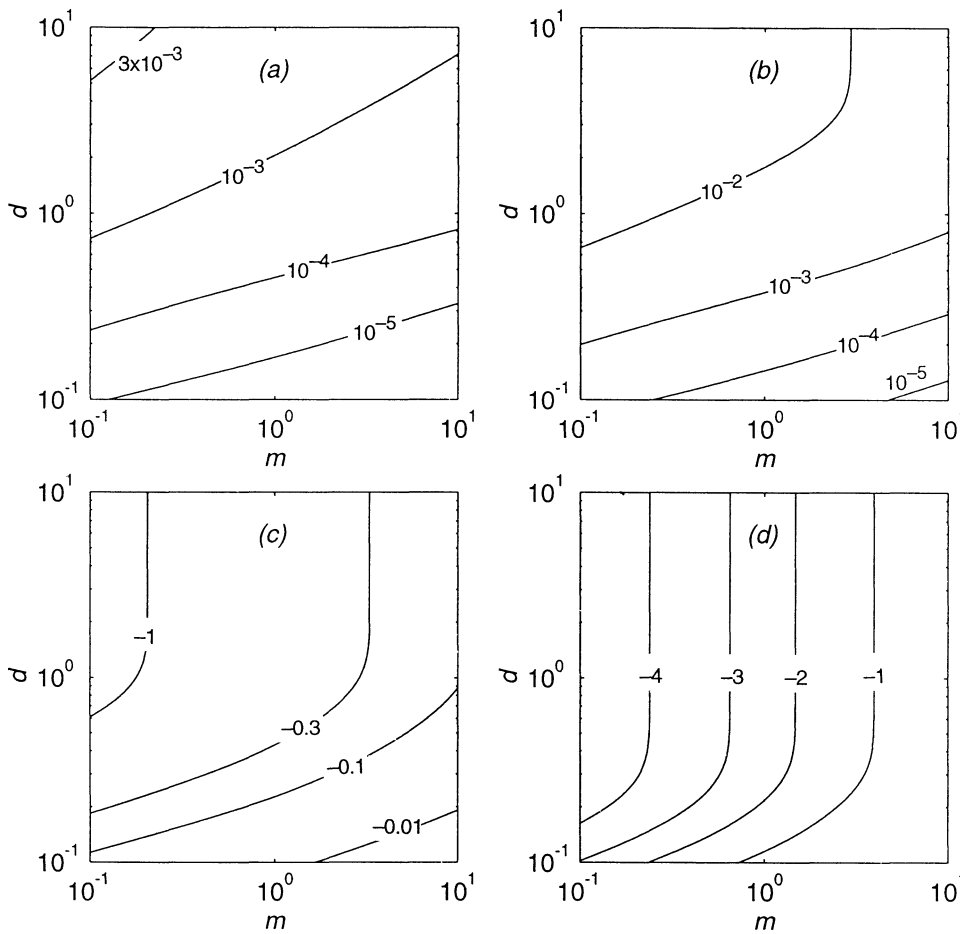

Figure 5. Isovalues of the growth rate (12) in the (m,d) plane for $\mathrm{Bo}=-1$ and $\mathrm{Ca}=1$. (a) $\alpha_1=0.1$; (b) $\alpha_1=0.9$; (c) $\alpha_1=3$; (d) $\alpha_1=10$ ($\alpha_1=1$ is neutral).

3.2. Weak gravity and surface tension effects: $\mathrm{We} \gg 1$, $\mathrm{Fr} \gg 1$

In this section, gravity and surface tension effects are assumed to be much weaker than inertia, i.e. $\mathrm{We} \gg 1$ and $\mathrm{Fr} \gg 1$. The zeroth-order conservation equations and boundary conditions are the same as previously, except for the normal stress interfacial condition whose right-hand side is now zero. The eigenvalue is real, and gives the wave velocity (11) with a zero growth rate.

At first-order, the momentum equations involve the inertia terms. The general solution of the homogeneous equations satisfying the conservation equations and the no-slip conditions at the walls has the same form as the zeroth-order solution (10), with new integration constants C_j and D_j in place of A_j and B_j:

$$i\hat{v}_{jg}^{(1)} = (C_j Y_j - D_j)\mathrm{sh}\, Y_j + D_j Y_j \mathrm{ch}\, Y_j, \tag{18a}$$

$$\hat{u}_{jg}^{(1)} = i\partial_y \hat{v}_{jg}^{(0)} = (D_j Y_j + C_j)\mathrm{sh}\, Y_j + C_j Y_j \mathrm{ch}\, Y_j, \tag{18b}$$

$$i\hat{p}_{jg}^{(1)} = 2m_j\alpha_1^2(C_j \mathrm{sh}\, Y_j + D_j \mathrm{ch}\, Y_j). \tag{18c}$$

A particular solution, satisfying the conservation equations and the no-slip conditions at the walls, is found to be:

$$\begin{aligned}\hat{v}_{jp}^{(1)} = \frac{r_j}{12m_j^2\alpha_1^2} Y_j^2 \big(&(B_j Y_j - 3A_j - 3(m_j c_0 + \delta_j \alpha_j) B_j)\mathrm{sh}\, Y_j \\ &+ (A_j Y_j - 3B_j - 3(m_j c_0 + \delta_j \alpha_j) A_j)\mathrm{ch}\, Y_j \big),\end{aligned} \tag{19a}$$

$$\hat{u}_{jp}^{(1)} = i\partial_y \hat{v}_{jp}^{(0)}, \tag{19b}$$

$$\begin{aligned}\hat{p}_{jp}^{(1)} = -\frac{r_j}{2m_j} \big(&(B_j Y_j^2 + A_j Y_j + 4B_j + (m_j c_0 + \delta_j \alpha_j) A_j)\mathrm{sh}\, Y_j \\ &+ (A_j Y_j^2 - 3B_j Y_j + 2A_j + 3(m_j c_0 + \delta_j \alpha_j) B_j)\mathrm{ch}\, Y_j \big),\end{aligned} \tag{19c}$$

with $\delta_1 = 1$ and $\delta_2 = -1$, where c_0 is given by (11) and A_j and B_j are given in Appendix 1.

The integration constants C_j and D_j are found from the four interfacial boundary conditions. These conditions may be written under matrix form $MX_1 = b_1$, where $X_1 = (C_1, D_1, C_2, D_2)$, M is the same as at zeroth-order, and b_1 is given in Appendix 2. The kinematic condition then gives the eigenvalue $c^{(1)}$; this eigenvalue is imaginary, $c^{(1)} = ic_i$, and gives the growth rate $\sigma_1 = \mathrm{Re}\, c_i$:

$$\begin{aligned}\sigma_1 = \mathrm{Re}\, \hat{v}_1^{(1)}(0) = \mathrm{Re} \Big\{ &-i\big((C_1\alpha_1 - D_1)\mathrm{sh}\,\alpha_1 + D_1\alpha_1 \mathrm{ch}\,\alpha_1\big) \\ &- \frac{1}{12}\big((3A_1 + (3c_0 + 2\alpha_1)B_1)\mathrm{sh}\,\alpha_1 + (3B_1 + (3c_0 + 2\alpha_1)A_1)\mathrm{ch}\,\alpha_1\big)\Big\}.\end{aligned} \tag{20}$$

In the long wave limit ($\alpha_1 \to 0$, fixed d), the growth rate is given by:

$$\sigma_1 \sim \alpha_1^2 \mathrm{Re}\,(1-m)\big(\mathrm{P}_0(m,d) + r\mathrm{P}_1(m,d)\big), \quad \alpha_1 \to 0, \tag{21}$$

where $\mathrm{P}_0(m,d)$ and $\mathrm{P}_1(m,d)$ are polynomial expressions given in Appendix 2. This is exactly the long wave result of Yih [1] ($\alpha_1 \ll 1$, $\mathrm{Re} = \mathrm{O}(1)$). Omitting the complicated dependence upon the parameters m, d and

r, the growth rate σ_1 scales as $\alpha_1^2 \mathrm{Re}(1-m) = \rho_1 a_1 k^2 h_1^4 (\mu_1 - \mu_2)/\mu_1^2$, proportional to small inertial effects of order $\alpha_1 \mathrm{Re}$.

In the short wave limit ($\alpha_1 \to \infty$, fixed d), the growth rate tends to:

$$\sigma_1 \sim \frac{\mathrm{Re}}{\alpha_1^2} \frac{(1-m)(r-m^2)}{2m^2(1+m)^2}, \quad \alpha_1 \to \infty. \tag{22}$$

This is exactly the short wave result of Hooper and Boyd [3] ($\alpha_1^2/\mathrm{Re} \gg 1$). It corresponds to a growth rate $\sigma_1 \sim \mathrm{Re}/\alpha_1^2 = a_1/k^2\nu_1$, proportional to small inertial effects of order Re/α_1^2 [4]. In particular, (22) shows that short waves are always unstable when the densities are equal ($r = 1$).

Figures 6 and *7* display the four types of variations of the growth rate (20) versus wavenumber α_1, along with the long wave and short wave expressions (21) and (22). *Figure 6* shows 'short wave instability', and *figure 7* shows 'short wave stability', the latter corresponding to $r < m^2 < 1$ or $r > m^2 > 1$. *Figures 6(a)* and *7(a)* show 'long wave instability', which typically occurs when the thinner layer is the more viscous [2], whereas *figures 6(b)* and *7(b)* show 'long wave stability', which typically occurs when the thinner layer is the less viscous. Finally, it appears that growth rate curves simply connect the asymptotic curves for long and short waves.

More complete information can be gained from *figure 8* which displays isovalues of the growth rate (20) in the (m, d) plane for $r = 1$, for four values of the wavenumber. These plots show that the instability domains expand as the wavenumber increases. For unequal densities ($r \neq 1$), *figure 8* remains qualitatively the same, except that for short waves there remains a vertical stable band for $r^{1/2} < m < 1$ when $r < 1$, or for $1 < m < r^{1/2}$ when $r > 1$. *Figure 8* also shows that the growth rate no longer depends on d for $d > 4/\alpha_1$, i.e. for $\alpha_2 > 4$, which means that a wall does not play any role as soon as the wavelength is less than 1.5 times the thickness of the fluid layer.

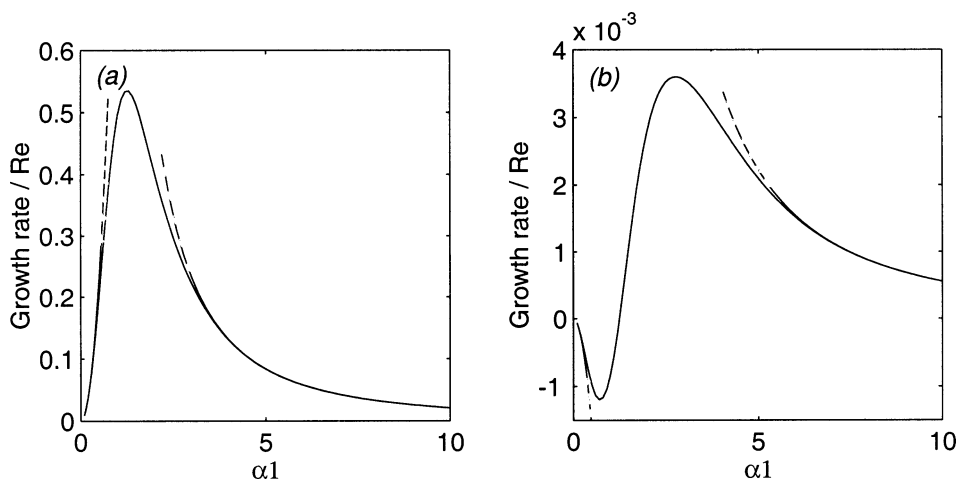

Figure 6. Growth rate σ_1/Re (20) (plain curves), and long wave (21) and short wave (22) results (dashed curves), for (a) $m = 0.3$ and (b) $m = 3$. $d = 3$, $r = 1$, $\mathrm{Fr} = \infty$ and $\mathrm{We} = \infty$.

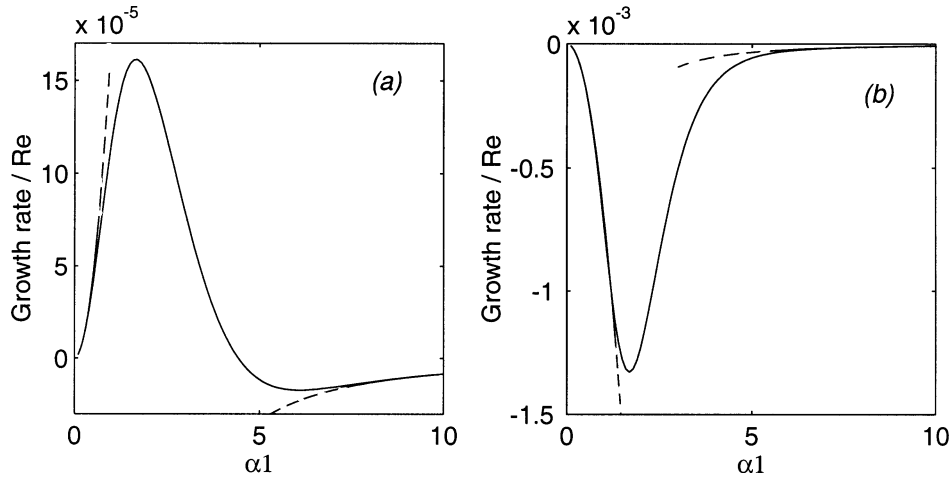

Figure 7. Growth rate σ_1/Re (20) (plain curves), and long wave (21) and short wave (22) results (dashed curves), for (a) $d = 0.9$; (b) $d = 2$. $m = 1.1$ and $r = 1.3$, $\mathrm{Fr} = \infty$ and $\mathrm{We} = \infty$.

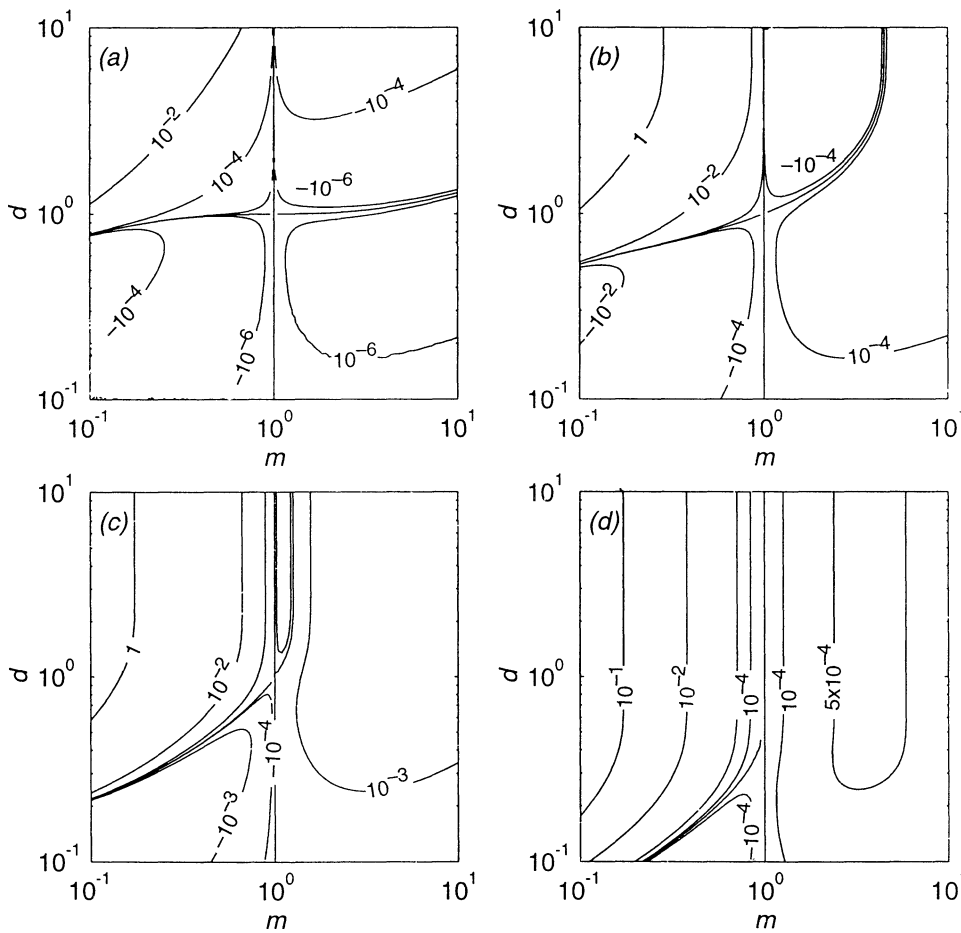

Figure 8. Isovalues of the growth rate σ_1 (20) in the (m, d) plane for (a) $\alpha_1 = 0.1$; (b) $\alpha_1 = 1$; (c) $\alpha_1 = 3$; (d) $\alpha_1 = 10$. $r = 1$, $\mathrm{Fr} = \infty$ and $\mathrm{We} = \infty$.

3.3. *Moderate gravity and surface tension effects:* $\mathrm{We} = \mathrm{O}(1)$, $\mathrm{Fr} = \mathrm{O}(1)$

We consider here the case of moderate gravity and surface tension effects, i.e. $\mathrm{We} = \mathrm{O}(1)$ and $\mathrm{Fr} = \mathrm{O}(1)$. Hence the inertial instability, essentially governed by the viscosity difference, may compete with the Rayleigh–Taylor instability, itself essentially governed by the density difference. The zeroth-order equations give the wave velocity (11). The first-order equations are the same as in the previous section, except that the normal stress interfacial condition involves the gravity and surface tension terms. Since the equations to be solved are linear, the growth rate is simply the sum of σ_0, given by (12) and σ_1, given by (20):

$$\sigma = \sigma_0 + \sigma_1. \tag{23}$$

For high wavenumbers, σ_0 scales as $-k$, and σ_1, as $\pm k^{-2}$, so that the growth rate is always dominated by the stabilising effect of surface tension, i.e. $a_1\sigma \sim -k\gamma/(\mu_1+\mu_2)$. The case of small wavenumbers is richer, since both the density and viscosity differences may be stabilising or destabilising. Only the two most interesting situations are considered here, namely those when increasing the shear rate leads to complete stabilisation or destabilisation of the flow. The physical situation of interest is the effect of an increase of the shear rate for given fluids and layer thicknesses; thus, we introduce the Galileo number $\mathrm{Ga} := \mathrm{Re}^2/\mathrm{Fr} = (1-r)\rho_1^2 g h_1^3/\mu_1^2$ which does not depend on the shear rate, so that varying the Reynolds number amounts to varying the shear rate a_1 with the other dimensionless parameters fixed.

The first remarkable situation is depicted in *figure 9*, which shows how a flow unstable to gravity ($r > 1$), may be completely stabilised by inertia as the Reynolds number is increased beyond some critical value Re_c; for the parameters of *figure 9*, $\mathrm{Re}_c = 0.6816$. For $\mathrm{Re} < \mathrm{Re}_c$, the Rayleigh–Taylor instability dominates and the flow is unstable to long waves (*figures 9(a)* and *(b)*). For $\mathrm{Re} > \mathrm{Re}_c$, the stabilising effect of inertia dominates, and the flow is stable to all wavenumbers (*figures 9(c)* and *(d)*). This situation typically occurs when the thinner layer is the less viscous. The critical Reynolds number corresponds to the change of concavity of the long wave parabola (dashed curves), and is obtained by writing $\sigma_0 + \sigma_1 = 0$ with σ_0 given by (16) and σ_1 given by (21):

$$\mathrm{Re}_c^2 = \frac{\mathrm{Ga}}{(1-m)}\frac{S(m,d)}{\mathrm{P}_0(m,d) + r\mathrm{P}_1(m,d)}.$$

This critical situation corresponds to a balance between inertia and gravity, and may be more properly defined by the critical (negative) Froude number:

$$\mathrm{Fr}_c = \frac{\mathrm{Re}_c^2}{\mathrm{Ga}} = \frac{S(m,d)}{(1-m)(\mathrm{P}_0(m,d) + r\mathrm{P}_1(m,d))}. \tag{24}$$

The second remarkable situation, depicted in *figure 10*, corresponds to a gravity-stable arrangement of the fluid layers ($r < 1$). For the flow parameters of *figure 10*, the growth rate curve merges in the Rayleigh–Taylor curve as long as $\mathrm{Re} < 0.1$ (which corresponds to $\mathrm{Fr} < 1$ and $\mathrm{We} < 1$). For higher Re, inertial effects stabilise long waves and destabilise short waves (*figures 10(a)* and *(b)*). Intermediate wavenumbers, for which the stabilising effect of surface tension is weak, are the most amplified (*figure 10(c)*). Instability then arises for a 'finite'critical Reynolds number $\mathrm{Re}_c = 0.9180$, with 'finite' wavenumber $\alpha_{1c} = 2.075$ (*figure 10(d)*). This situation has been pointed out numerically by Renardy and Renardy [16] and Sangalli et al. [11], and it appears from the present small-Re expansion that it occurs over a wide range of parameter values, when short waves are unstable (without surface tension) and long waves are stable with respect to both gravity ($r \leqslant 1$) and inertia effects (i.e. when the thinner layer is the less viscous). No simple expression for Re_c and α_{1c} can be given, but

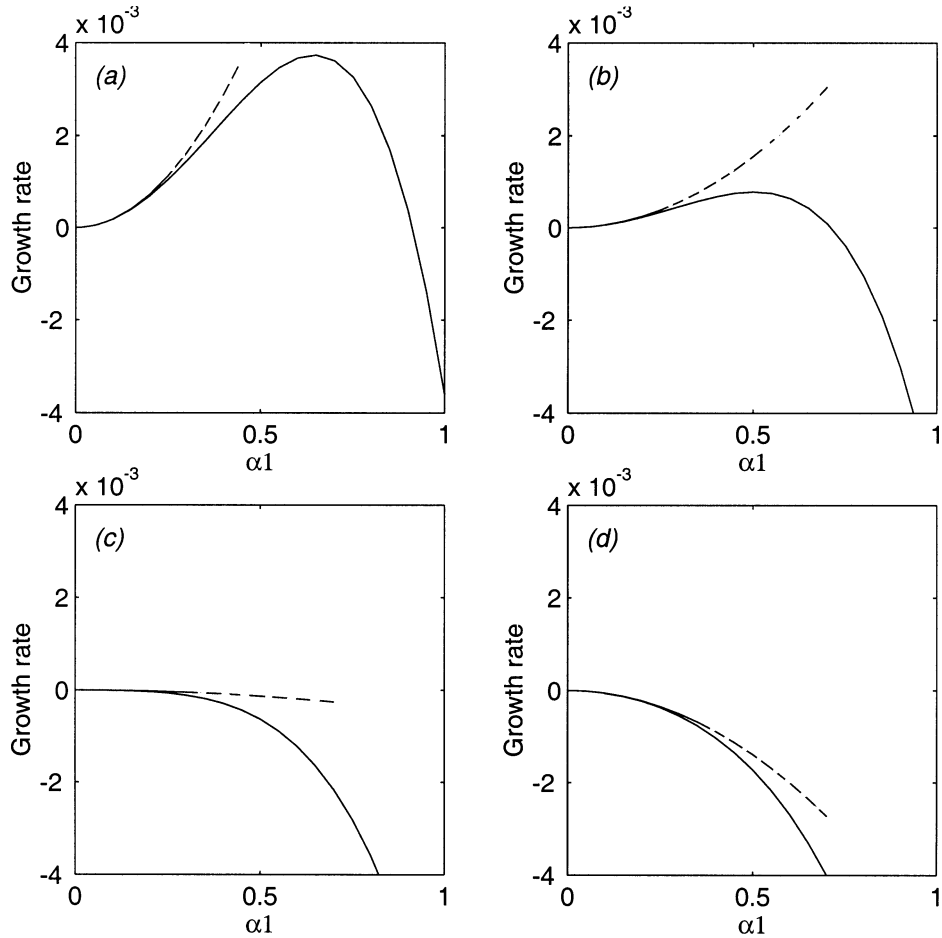

Figure 9. Growth rate σ (23) (plain curves) for (a) Re = 0.3; (b) Re = 0.5; (c) Re = 0.7; (d) Re = 0.9 and long wave result (- - -) (We $= -$Fr $=$ 0.09, 0.49, 0.81, 1). $m = 0.1$, $d = 0.2$, $r = 1.1$, Bo $= -1$ and Ga $= -1$. Complete stabilisation arises for $\mathrm{Re}_c = 0.6816$.

a crude relation between them can be obtained by writing $\sigma_0 + \sigma_1 = 0$ with σ_0 given by (17) and σ_1 given by (22), leading to:

$$\mathrm{Re}_c^2 \approx \frac{\alpha_{1c}^3 \mathrm{Ga}}{\mathrm{Bo}} \frac{m^2(1+m)}{(1-m)(r-m^2)}. \tag{25}$$

This critical situation corresponds to a balance between inertia and surface tension, and is more properly defined by the critical Weber number:

$$\mathrm{We}_c \approx \alpha_{1c}^3 \frac{m^2(1+m)}{(1-m)(r-m^2)}. \tag{26}$$

In the two examples discussed above, the small-Re expansion has been assumed to remain valid up to Re ≈ 1. As shown in the next section, this is true with typical error smaller than 1%, at least for m, d and r in the range 0.1–10.

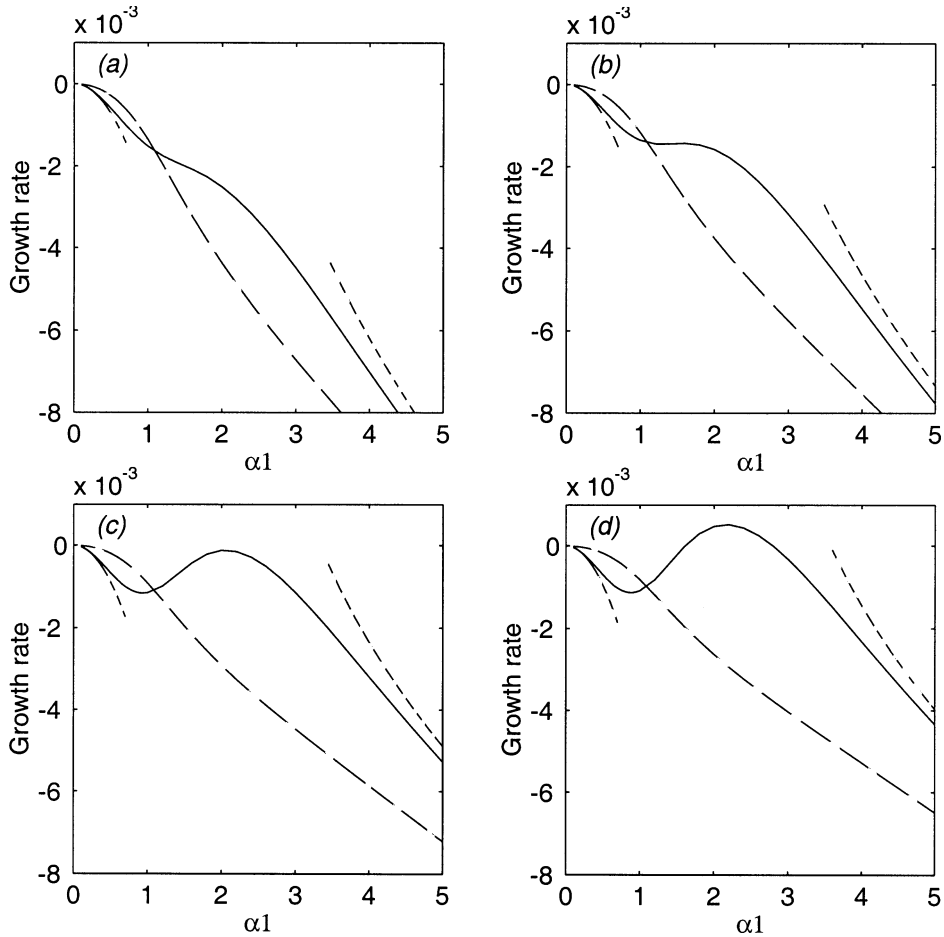

Figure 10. Growth rate σ/Re (plain curves) for (a) $\mathrm{Re} = 0.6$; (b) $\mathrm{Re} = 0.7$; (c) $\mathrm{Re} = 0.9$; (d) $\mathrm{Re} = 1$ ($\mathrm{We} = \mathrm{Fr} = 36, 49, 81, 100$). The Rayleigh–Taylor growth rate (12) (— — —), and long and short wave results (- - -) are also shown in each figure. $m = 3$, $d = 2$, $r = 0.8$, $\mathrm{Bo} = 1$ and $\mathrm{Ga} = 0.01$.

4. Validity domain of the small-Re expansion

In order to check the validity domain of the small-Re expansion, the Orr–Sommerfeld equations and boundary conditions (7)–(8) have been solved numerically. The numerical method is based on the classical expansion of the eigenfunctions in Chebyshev polynomials [28]. The numerical code [29] has been checked using symmetries as well as asymptotic and numerical results [8,9,15].

Figures 11 and *12* compare the small-Re wave velocity (11) and growth rate (20) to the numerical solution, for parameters given in the captions. These figures also display the long wave and short wave results of Yih [1] and Hooper and Boyd [3]. For the wave velocity, the small-Re and numerical curves are merged for $\mathrm{Re} < 1$, and it can be seen that their difference remains small even for $\mathrm{Re} = 10$. However, the log-log plot in *figure 12* shows that the relative error of the small-Re result (20) (which is actually a creeping flow result) grows for high wavenumbers, whereas Hooper and Boyd's result [3] gives the right algebraic decay for small but finite inertia effects, as already discussed in the previous section. For the growth rate, the maximum difference remains very small for $\mathrm{Re} < 1$, and the asymptotic growth rate (20) remains qualitatively good for $\mathrm{Re} = 10$. *Table I* gives the maximum error on the asymptotic growth rate for $\mathrm{Re} = 1, 3$ and 10, for the parameters of *figures 11* and *12*.

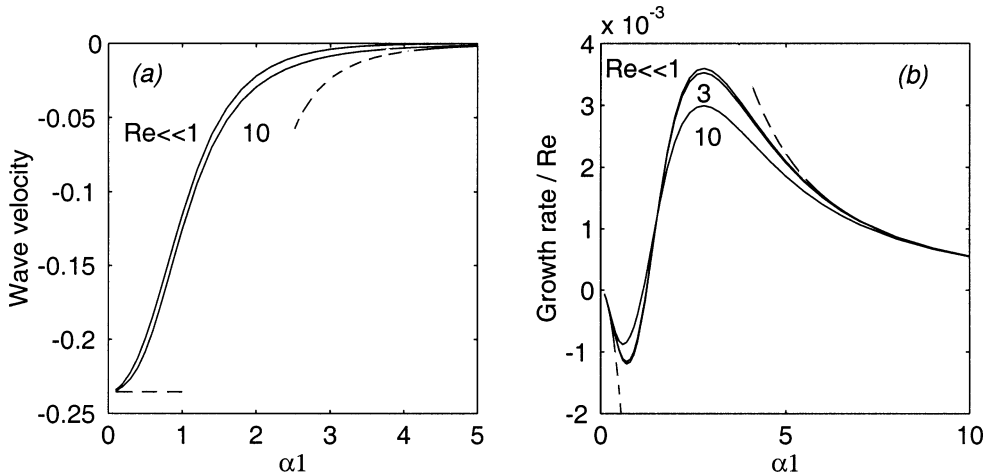

Figure 11. (a) Wave velocity $c^{\dim}/a_1h_1$: small-Re result (11) and numerical result for $\mathrm{Re} = 10$; (b) growth rate σ/Re: small-Re result (20) and numerical result for $\mathrm{Re} = 3$ and 10. Dashed curves: long wave and short wave results. $m = 3$, $d = 3$, $r = 1$, $\mathrm{Fr} = \infty$ and $\mathrm{We} = \infty$.

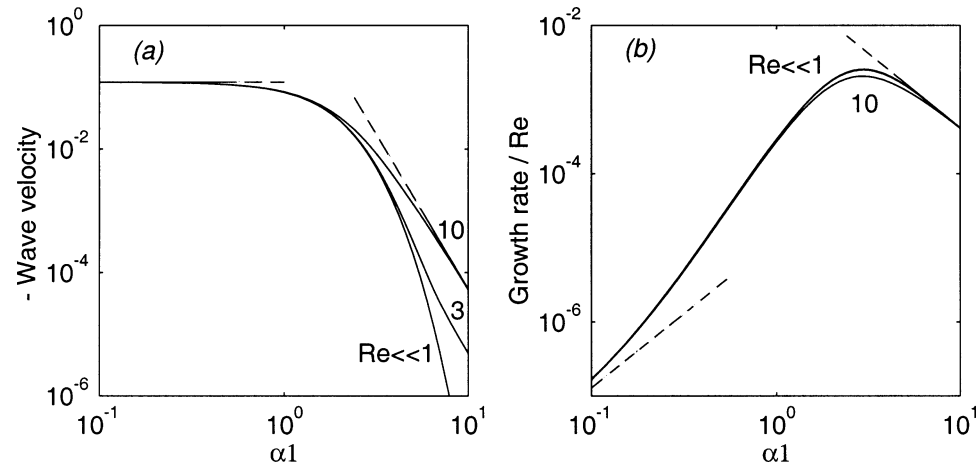

Figure 12. (a) Wave velocity $-c^{\dim}/a_1h_1$: small Re result (11) and numerical result for $\mathrm{Re} = 3$ and 10; (b) growth rate σ/Re: small Re result (20) and numerical result for $\mathrm{Re} = 10$. Dashed lines: long wave and short wave results. $m = 2$, $d = 1$, $r = 1$, $\mathrm{Fr} = \infty$ and $\mathrm{We} = \infty$.

Table I. Relative maximum difference between the small-Re growth rate (20) and the numerical solution, for $\mathrm{Re} = 1, 3$ and 10. Flow parameters are given in the captions of *figures 11* and *12*.

	$\mathrm{Re} = 1$	$\mathrm{Re} = 3$	$\mathrm{Re} = 10$
Parameters of *figure 11*	0.25%	2.25%	24.1%
Parameters of *figure 12*	0.35%	3.16%	36.8%

Other comparisons have been made, including the effect of surface tension and gravity, which confirm that the maximum error remains less than 1% for $\mathrm{Re} < 1$.

When the Reynolds number is increased further, numerical investigation shows that the growth rate curves display a qualitatively new feature: moderate wavenumbers with $\alpha_1 = \mathrm{O}(1)$ stabilise, in agreement with the

'phase diagram' of interfacial instabilities proposed by Charru and Hinch [5]. This is illustrated on *figure 13*, which displays the wave velocity and growth rate for Re increasing from 10 to 100. It appears that beyond $\mathrm{Re} \approx 46.57$, a band of stable wavenumbers appears, centred around $\alpha_1 \approx 0.584$. This band, which typically occurs for Reynolds numbers of a few tenths for other flow parameters, broadens when the Reynolds number increases.

For still higher Reynolds numbers, typically of a few hundreds, a new instability arises for wavenumbers of order 1, in agreement with results of Renardy [8]; for the parameters of *figure 13*, the critical Reynolds number and wavenumber are $\mathrm{Re}_c = 228.95$ and $\alpha_{1c} = 0.527$. *Figure 14* displays typical variations of the growth rate versus Reynolds number for the two least stable modes, for the wavenumbers $\alpha_1 = 0.15$ and 0.3. The growth rate of the interfacial mode (*figure 14(a)*) first grows linearly, then decreases and becomes negative as previously discussed; however, for $\alpha_1 = 0.3$ (resp. $\alpha_1 = 0.5$), the growth rate increases again and becomes positive for $\mathrm{Re} \approx 325$ (resp. $\mathrm{Re} \approx 613$). The second mode remains stable (*figure 14(b)*), with a growth rate independent of

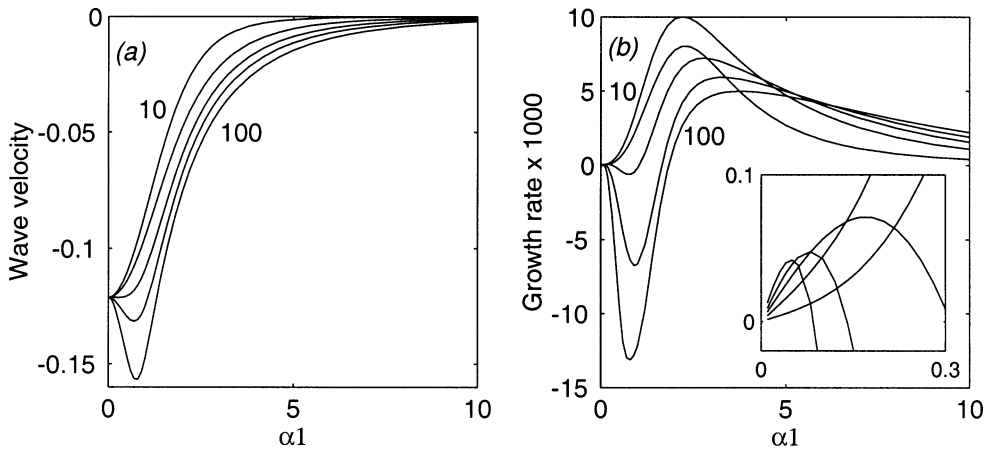

Figure 13. (a) Wave velocity $c^{\dim}/a_1 h_1$ and (b) growth rate σ/Re: numerical solution for $\mathrm{Re} = 10, 30, 50, 70$ and 100. $m = 2$, $d = 1$, $r = 1$, $\mathrm{Fr} = \infty$ and $\mathrm{We} = \infty$.

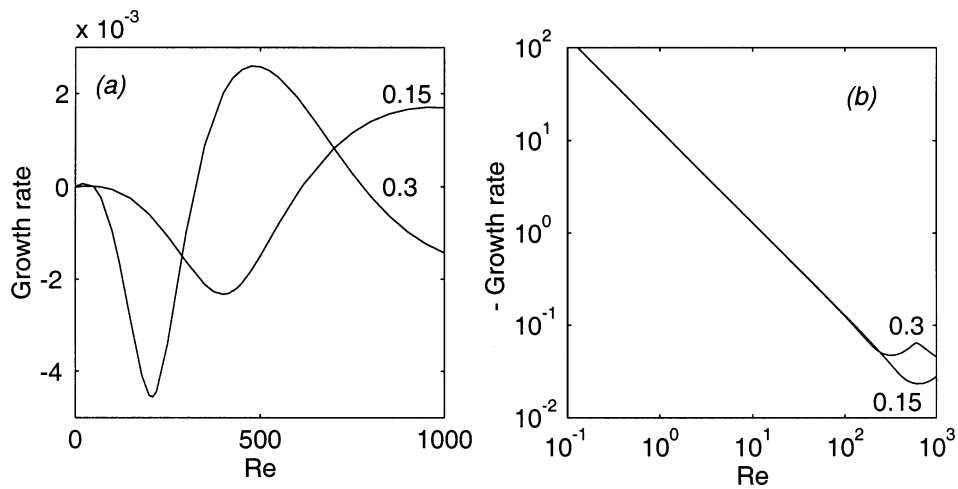

Figure 14. Growth rate versus Reynolds number of (a) the interfacial mode and (b) the least stable shear mode, for $\alpha_1 = 0.15$ and $\alpha_1 = 0.3$. $m = 2$, $d = 1$, $r = 1$, $\mathrm{Fr} = \infty$ and $\mathrm{We} = \infty$.

the wavenumber and varying as:

$$\sigma = \alpha c = -12.9/\mathrm{Re}. \tag{27}$$

The growth rate of this shear mode (or Tollmien–Schlichting mode) remains much smaller than that of the interfacial mode, and therefore these two modes do not cross. However, the nature of the instability has changed, as shown below from the shape of the eigenfunctions and energy analysis.

5. Nature of the instability

Figure 15 displays the real and imaginary parts of the eigenfunctions $\hat{u}$, $\hat{v}$ and $\hat{\omega}$, for $\alpha_1 = 1$ and $\mathrm{Re} = 1$, with the normalisation condition $\hat{\eta} = 1$ (thus the real part of the eigenfunctions is in phase with the interface). It can be seen that these eigenfunctions affect the whole thickness of the layers and exhibit their maximum at the interface. These shapes are typical of the interfacial mode, and remain similar for $\alpha_1 < 1$ and $\mathrm{Re} < 1$. The discontinuity of $\hat{u}$ corresponds to the continuity of the total velocity at the deformed interface (see (7a)). For higher wavenumbers (*figure 16*, $\alpha_1 = 10$), disturbances are more and more localised in the vicinity of the interface, with penetration depth of vorticity disturbances of order k^{-1} [4]. *Figure 17* displays the same

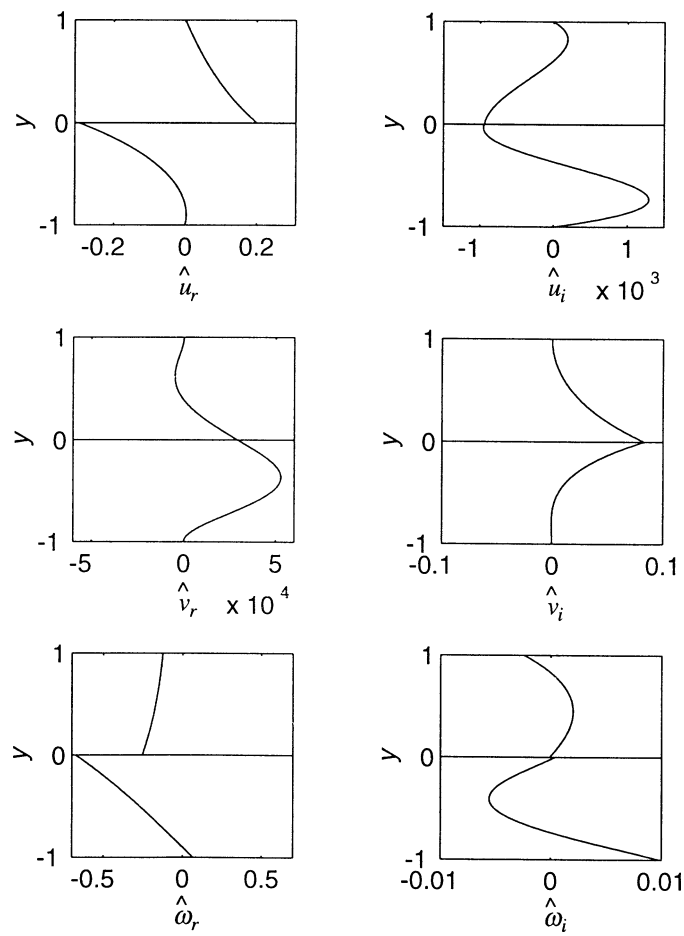

Figure 15. Eigenfunctions $\hat{u}_r$, $\hat{u}_i$, $\hat{v}_r$, $\hat{v}_i$, $\hat{\omega}_r$, $\hat{\omega}_i$ for $\alpha_1 = 1$, $\mathrm{Re} = 1$, $m = 2$, $d = 1$, $r = 1$, $\mathrm{Fr} = \infty$ and $\mathrm{We} = \infty$. $c = -0.083033$, $\sigma = 290.39 \times 10^{-6}$.

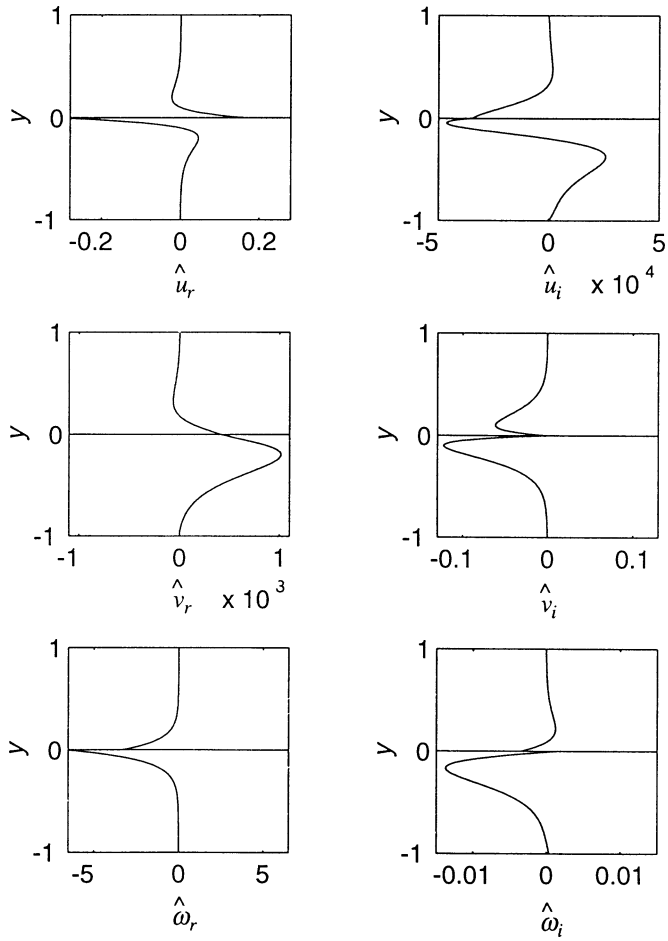

Figure 16. Eigenfunctions $\hat{u}_r$, $\hat{u}_i$, $\hat{v}_r$, $\hat{v}_i$, $\hat{\omega}_r$, $\hat{\omega}_i$ for $\alpha_1 = 10$, Re $= 1$, $m = 2$, $d = 1$, $r = 1$, Fr $= \infty$ and We $= \infty$. $c = -0.56027 \times 10^{-6}$, $\sigma = 41.656 \times 10^{-6}$.

eigenfunctions for $\alpha_1 = 0.3$ and Re $= 500$, i.e. in the range of unstable Reynolds numbers shown in *figure 14(a)*. It appears that these eigenfunctions are quite different from those of the interfacial mode at small Reynolds numbers: $\hat{u}$ is still discontinuous at the interface, but its maximum lies close to the walls, as for the classical shear modes of parallel shear flows [7,30]. Similarly, vorticity is concentrated near the walls, disturbances being nearly irrotational in the middle half of the channel.

Another characterisation of the nature of the instability can be obtained from the equation giving the energy budget of the disturbance. Multiplying the linearised Navier–Stokes equation by the velocity disturbance **u**, and integrating over one wavelength and over the thickness of the layers, one obtains [3,31–33]:

$$\mathrm{RKINE}\,j = \mathrm{REYNS}\,j + \mathrm{SHEST}\,j + \mathrm{NORST}\,j + \mathrm{DISSIP}\,j, \quad j = 1, 2, \tag{28}$$

where:

$$\mathrm{RKINE}\,j = \frac{r_j}{2}\frac{\mathrm{d}}{\mathrm{d}t}\int_{\Omega j}\left(u_j^2 + v_j^2\right)\mathrm{d}y\,\mathrm{d}x,$$

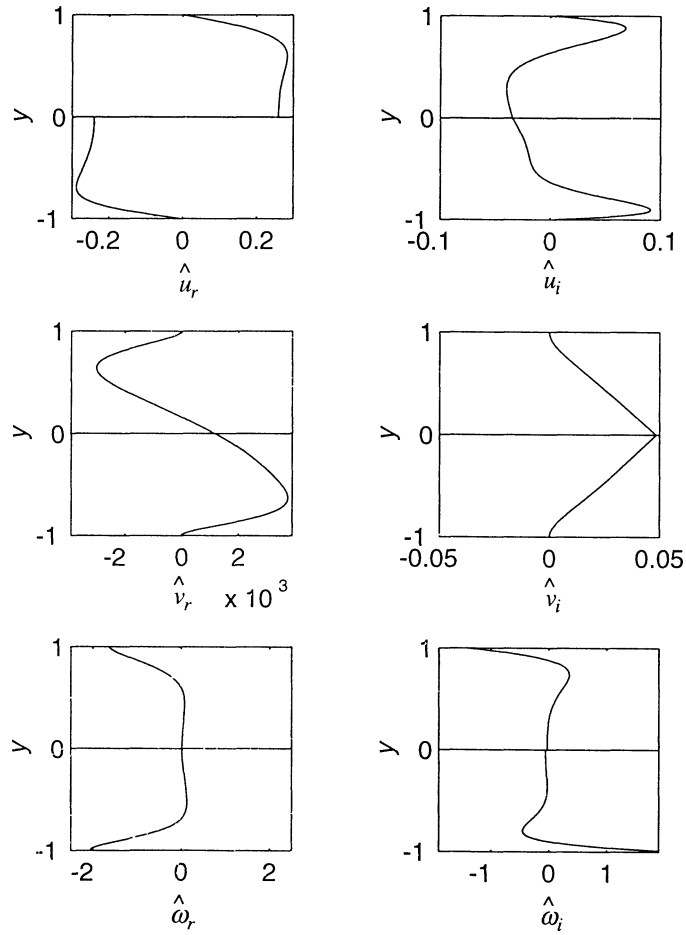

Figure 17. Eigenfunctions $\hat{u}_r, \hat{u}_i, \hat{v}_r, \hat{v}_i, \hat{\omega}_r, \hat{\omega}_i$ for $\alpha_1 = 0.3$, $\mathrm{Re} = 500$, $m = 2$, $d = 1$, $r = 1$, $\mathrm{Fr} = \infty$ and $\mathrm{We} = \infty$. $c = -0.23559$, $\sigma = 8614.6 \times 10^{-6}$.

$$\mathrm{REYNS}j = -r_j \int_{\Omega j} u_j v_j \partial_y \overline{U}_j \,\mathrm{d}y\,\mathrm{d}x,$$

$$\mathrm{SHEST}j = \delta_j \frac{m_j}{\mathrm{Re}} \int_{0,y=0}^{2\pi} (\partial_y u_j + \partial_x v_j) u_j \,\mathrm{d}x,$$

$$\mathrm{NORST}j = \delta_j \frac{1}{\mathrm{Re}} \int_{0,y=0}^{2\pi} (-p_j + 2m_j \partial_y v_j) v_j \,\mathrm{d}x,$$

$$\mathrm{DISSI}j = -\frac{m_j}{\mathrm{Re}} \int_{\Omega j} \left(2(\partial_x u_j)^2 + (\partial_y u_j + \partial_x v_j)^2 + 2(\partial_y v_j)^2\right) \mathrm{d}y\,\mathrm{d}x$$

with $\Omega_1 = [0, 2\pi] \times [-\alpha_1, 0]$, $\Omega_2 = [0, 2\pi] \times [0, \alpha_2]$, and $\delta_1 = 1$, $\delta_2 = -1$. RKINEj is the rate of change of the kinetic energy of the disturbances, REYNSj is the energy transfer from the mean flow to the disturbances via the Reynolds stresses, DISSIj is the rate of viscous dissipation, and NORSTj and SHESTj are the rate of work of normal and tangential stresses due to the perturbations at the interface. Taking into account the continuity of

velocity and stress at the interface, the sum of the rates of work of normal stresses can be written as:

$$\mathrm{NORST1} + \mathrm{NORST2} = -\mathrm{HYDPR} - \mathrm{SURTE}, \tag{29}$$

where:

$$\mathrm{HYDPR} = \frac{1}{\mathrm{Fr}} \int_0^{2\pi} \eta \partial_t \eta \, \mathrm{d}x,$$

$$\mathrm{SURTE} = -\frac{1}{\mathrm{We}} \int_{0,\, y=0}^{2\pi} \partial_{xx} \eta \partial_t \eta \, \mathrm{d}x,$$

represent the rates of change of the gravitational potential energy and of the interfacial potential energy, respectively. Summing equations (28), one obtains the energy equation for both fluids:

$$\begin{aligned} &\mathrm{RKINE1} + \mathrm{RKINE2} + \mathrm{HYDPR} + \mathrm{SURTE} \\ &= \mathrm{REYNS1} + \mathrm{REYNS2} + \mathrm{SHEST1} + \mathrm{SHEST2} + \mathrm{DISSIP1} + \mathrm{DISSIP2}, \end{aligned} \tag{30}$$

where the left-hand side represents the mechanical energy of the flow.

Table II gives the values of these terms, normalised by DISSI1, for $\mathrm{Re} = 1$ and for $\alpha_1 = 0.1$, 1 and 10 (only the ratios of these terms, which depend neither on time nor on the normalisation condition, are relevant). It appears that the terms SHESTj and DISSIj are dominant, and that the term REYNSj is negligible. We have verified that this hierarchy holds for other values of the parameters as long as $\mathrm{Re} < 1$. Moreover, for $\alpha_1 \gg 1$, one finds that $\mathrm{DISSI1}/\mathrm{DISSI2} = \mathrm{SHEST1}/\mathrm{SHEST2} = m$, as predicted by Hooper and Boyd [3], equation (55) (the dissipation rate is greater in the less viscous fluid because velocity gradients are stronger there).

Table III gives the value of the terms of the energy equation (30), still normalised by DISSI1, for $\mathrm{Re} = 1000$ and for $\alpha_1 = 0.1$, 0.2 and 1. It appears here that the energy equation is dominated by the terms REYNSj and DISSIj, and that the SHESTj terms are now much smaller. Finally, *tables II* and *III* confirm, as expected, that the small-Re instability is fed by the rate of work of the interfacial stress, whereas the high-Re instability which corresponds to that studied by Hooper and Boyd [7], is fed by the Reynolds stresses.

Finally, the eigenvalues of the two-layer Couette flow may be compared to those of the single-layer Couette flow. *Table IV* shows that, putting the interfacial mode aside, the eigenvalues of the two-layer flow come close

Table II. Value of the terms of the kinetic energy equation (30) normalised by DISSI1, for $\mathrm{Re} = 1$, $m = 2$, $d = 1$, $r = 1$, $\mathrm{We} = \infty$, $\mathrm{Fr} = \infty$ (HYDPR = SURTE = 0). The terms NORSTj can be obtained from (28).

	$\alpha_1 = 0.1$	$\alpha_1 = 1$	$\alpha_1 = 10$
Wave velocity	−0.12075	−0.083033	−0.56027E-06
Growth rate	0.16739E-06	0.29039E-03	0.41656E-03
RKINE1	4.45E-08	2.02E-05	1.05E-06
RKINE2	4.02E-08	1.47E-05	2.60E-07
REYNS1	7.07E-06	2.10E-04	−3.18E-06
REYNS2	2.42E-06	2.09E-05	−9.73E-07
DISSI1	−1	−1	−1
DISSI2	−1.35	−0.891	−0.501
SHEST1	1.29	1.13	1.00
SHEST2	1.07	0.754	0.501

Table III. Value of the terms of the kinetic energy equation (28) for Re = 1000, $m = 2$, $d = 1$, $r = 1$, We = ∞, Fr = ∞ (HYDPR = SURTE = 0).

	$\alpha_1 = 0.1$	$\alpha_1 = 0.2$	$\alpha_1 = 1$
Wave velocity	−0.22825	−0.24231	−0.180
Growth rate	0.41617E-03	0.11607E-02	−0.784E-02
RKINE1	6.63E-02	1.25E-01	−5.00E-01
RKINE2	6.69E-02	1.26E-01	−5.03E-01
REYNS1	1.90	1.79	0.412
REYNS2	0.772	0.846	0.656
DISSI1	−1	−1	−1
DISSI2	−1.43	−1.38	−1.49
SHEST1	−5.03E-02	5.00E-03	2.25E-01
SHEST2	−5.43E-02	−1.08E-03	1.97E-01

Table IV. Comparison of the eigenvalues of the two-layer and one-layer Couette flow with same Reynolds number Re = 10000. The first line corresponds to the interfacial mode, and the other ones to the least stable shear modes. $\alpha_1 = 1$, $m = 10$, $d = 0.1$, $r = 1$, Bo = 0.

Two-layer flow, $m = 10$, We = ∞	Two-layer flow, $m = 100$, We = ∞	Two-layer flow, $m = 10$, We = 1	One-layer flow
$-0.01302 + i0.005305$	$-0.00168 + i0.00144$	$-0.2799 - i0.08974$	
$-0.169 - i0.0434$	$-0.185 - i0.0514$	$-0.188 - i0.0404$	$-0.186 - i0.0529$
$-0.813 - i0.0526$	$-0.814 - i0.0527$	$-0.813 - i0.0526$	$-0.814 - i0.0529$
$-0.267 - i0.111$	$-0.288 - i0.118$	$+0.159 - i0.114$	$-0.290 - i0.120$
$-0.709 - i0.111$	$-0.710 - i0.120$	$-0.709 - i0.120$	$-0.710 - i0.120$
$-0.351 - i0.139$	$-0.144 - i0.141$	$-0.131 - i0.133$	$-0.144 - i0.139$
$-0.856 - i0.167$	$-0.856 - i0.139$	$-0.856 - i0.139$	$-0.856 - i0.139$

to those of the corresponding one-layer flow when the second fluid is rigidified by increasing its viscosity or increasing surface tension. These eigenvalues of the one-layer and two-layer flows also come closer to each other when the viscosity and density ratios tend to unity, the interfacial mode becoming neutral.

6. Discussion and conclusion

The first aim of this paper was to unify previous results on the stability of the two-layer Couette flow from a small-Re expansion. From this expansion, the growth rate and wave velocity have been derived explicitly, for any wavenumber and physical parameter values. The long wave and short wave results of Yih [1] and Hooper [3] have been retrieved as special cases. The small-Re expansion emphasizes the fact that interfacial instability arises from small inertial effects acting on the disturbances created at the perturbed interface, for both long and short waves, in agreement with the physical mechanisms given by Hinch [4] and Charru and Hinch [5]. Note that for finite amplitude disturbances, numerical computations of two-layer Stokes flow indicates that disturbances are damped with wave velocity and growth rate equal to those predicted by the linear theory [24], for an amplitude to wall separation ratio higher than 10%, if surface tension is strong enough.

In addition to the small-Re expansion, the Orr–Sommerfeld equations have been solved numerically, in order to evaluate the validity domain of the various asymptotic results. Although the bounds of the validity domains depend on the viscosity and thickness ratios, and to a lesser extent to the density ratio, it has been shown that the long wave asymptotics give accurate results as soon as $kh_{\min} < 0.2$, where $h_{\min} = \min(h_1, h_2)$. On the other hand, the short wave asymptotics can be used as soon as $kh_{\min} > 4$, i.e. a wall does not play any role as soon as the wavelength is less than 1.5 times the thickness of the fluid layers. Finally, the validity domain of the small-Re expansion extends up to $\mathrm{Re} = 1$, with error smaller than 1%, and it gives qualitatively good results up to $\mathrm{Re} \approx 30$.

Gravity and surface tension effects have then been investigated. When these effects dominate over inertia effects (Weber number $\mathrm{We} \ll 1$ and Froude number $\mathrm{Fr} \ll 1$), the Rayleigh–Taylor instability dominates, with waves propagating with the flow of the less viscous fluid. When these effects are negligible ($\mathrm{We} \gg 1$ and $\mathrm{Fr} \gg 1$), the inertial instability discussed above dominates. When the Rayleigh–Taylor and inertial instabilities compete ($\mathrm{We} = \mathrm{O}(1)$ and $\mathrm{Fr} = \mathrm{O}(1)$), two situations appear noticeable. The first one corresponds to complete stabilisation of the Rayleigh–Taylor instability ($r > 1$) by inertia. It typically occurs when the thinner layer is the less viscous. Marginal stability corresponds to the balance between gravity and inertia, with finite critical Froude number Fr_c given by (24). The second noticeable situation corresponds to destabilisation of a gravity-stable flow ($r < 1$) by inertial effects, with finite critical wavenumber k_c. Renardy [8] first illustrated this situation numerically, and we gave here general conditions for its occurence. Marginal stability corresponds to the balance between surface tension and inertia, with finite critical Weber number We_c; although no simple marginal stability criterion was found, We_c and k_c are linked by (26).

Finally, higher Reynolds numbers were investigated numerically. For $\mathrm{Re} < 1$, the curve giving the growth rate versus wavenumber smoothly joins the long wave ($\sigma \sim \pm \mathrm{Re}\,\alpha_1^2$) and short wave ($\sigma \sim \pm \mathrm{Re}/\alpha_1^2$) asymptotic curves. For Re of a few tenths, inertia stabilises wavenumbers $\alpha_1 = \mathrm{O}(1)$. When Re is increased beyond a few hundreds, a new instability arises, with all the features of the classical shear mode of instability, as shown by Hooper and Boyd [7] (see also [34]). Looking at the eigenfunctions shows that their maximum no longer lies near the interface but near the walls; moreover, the dominant source term for the kinetic energy of the perturbations no longer comes from the rate of work of viscous stresses at the interface, but from Reynolds stresses within the bulk of the flow, in agreement with previous studies [33]. However, we have shown that for Couette flow, this instability corresponds to the same interfacial mode as for $\mathrm{Re} \ll 1$, and no mode crossing occurs. Indeed, the other damped modes remain far away from the interfacial mode (in the context of a thin film sheared by a high Reynolds number boundary layer, Timoshin [22] also emphasizes that the constant-shear approximation for the basic-flow predicts only interfacial instability). These damped modes correspond to the stable shear modes of the single-fluid Couette flow: when surface tension or the viscosity of one of the fluids is increased, the interface rigidifies, and the eigenvalues of the two-layer flow get closer to those of the corresponding single-layer flow. However, for high Reynolds number, small curvature of the velocity profile gives rise to unstable shear modes, which may interact strongly with the interfacial mode [22].

Appendix 1. Zeroth-order solution

At zeroth-order, the four interfacial conditions (7) lead to the matrix system $MX_0 = b_0$, where $X_0 = (A_1, B_1, A_2, B_2)$, and:

$$b_0 = \left(\frac{1-m}{m}, 0, 0, \frac{i}{2} \frac{\mathrm{Bo} + \alpha_1^2}{\alpha_1 \mathrm{Ca}} \right),$$

$$M = \begin{bmatrix} \operatorname{sh}\alpha_1 + \alpha_1 \operatorname{ch}\alpha_1 & \alpha_1 \operatorname{sh}\alpha_1 & \operatorname{sh}\alpha_2 + \alpha_2 \operatorname{ch}\alpha_2 & -\alpha_2 \operatorname{sh}\alpha_2 \\ \alpha_1 \operatorname{sh}\alpha_1 & -\operatorname{sh}\alpha_1 + \alpha_1 \operatorname{ch}\alpha_1 & -\alpha_2 \operatorname{sh}\alpha_2 & -\operatorname{sh}\alpha_2 + \alpha_2 \operatorname{ch}\alpha_2 \\ \operatorname{ch}\alpha_1 + \alpha_1 \operatorname{sh}\alpha_1 & \alpha_1 \operatorname{ch}\alpha_1 & -m(\operatorname{ch}\alpha_2 + \alpha_2 \operatorname{sh}\alpha_2) & m\alpha_2 \operatorname{ch}\alpha_2 \\ \alpha_1 \operatorname{ch}\alpha_1 & -\operatorname{ch}\alpha_1 + \alpha_1 \operatorname{sh}\alpha_1 & m\alpha_2 \operatorname{ch}\alpha_2 & m(\operatorname{ch}\alpha_2 - \alpha_2 \operatorname{sh}\alpha_2) \end{bmatrix}. \tag{A1}$$

The coefficients of the zeroth-order solution (10) are:

$$A_1 = \frac{1-m}{D}\big((\operatorname{ch}\alpha_1 - \alpha_1 \operatorname{sh}\alpha_1)(\operatorname{sh}2\alpha_2 - 2\alpha_2) + 2m\big(\operatorname{ch}^2\alpha_2 + \alpha_2^2\big)(\operatorname{sh}\alpha_1 - \alpha_1 \operatorname{ch}\alpha_1) + 2\alpha_1\alpha_2^2 \operatorname{ch}\alpha_1\big), \tag{A2}$$

$$B_1 = \frac{1-m}{D}\big(\alpha_1 \operatorname{ch}\alpha_1(\operatorname{sh}2\alpha_2 - 2\alpha_2) + 2m\alpha_1 \operatorname{sh}\alpha_1\big(\operatorname{ch}^2\alpha_2 + \alpha_2^2\big) - 2\alpha_2^2(\operatorname{ch}\alpha_1 + \alpha_1 \operatorname{sh}\alpha_1)\big),$$

$$A_2(\alpha_1, \alpha_2, m) = -\frac{1}{m} A_1(\alpha_2, \alpha_1, 1/m),$$

$$B_2(\alpha_1, \alpha_2, m) = \frac{1}{m} B_1(\alpha_2, \alpha_1, 1/m),$$

with

$$D = 2m^2\big(\operatorname{sh}^2\alpha_1 - \alpha_1^2\big)\big(\operatorname{ch}^2\alpha_2 + \alpha_2^2\big) + 2\big(\operatorname{ch}^2\alpha_1 + \alpha_1^2\big)\big)\big(\operatorname{sh}^2\alpha_2 - \alpha_2^2\big) + m\big(\operatorname{sh}2\alpha_1 \operatorname{sh}2\alpha_2 + 4\alpha_1^2\alpha_2^2 - 4\alpha_1\alpha_2\big).$$

Appendix 2. First-order solution

The four interfacial conditions lead to the matrix system $MX_1 = b_1$, where $X_1 = (C_1, D_1, C_2, D_2)$, M is given by (A1) and:

$$b_1 = \begin{bmatrix} \hat{u}_{2p}^{(1)} - \hat{u}_{1p}^{(1)} \\ i\big(\hat{v}_{2p}^{(1)} - \hat{v}_{1p}^{(1)}\big) \\ m\big(\partial_y \hat{u}_{2p}^{(1)} + i\hat{v}_{2p}^{(1)}\big) - \big(\partial_y \hat{u}_{1p}^{(1)} + i\hat{v}_{1p}^{(1)}\big) \\ \dfrac{1}{2i}\big(\hat{p}_{2p}^{(1)} - \hat{p}_{1p}^{(1)} - 2m\partial_y \hat{v}_{2p}^{(1)} + 2\partial_y \hat{v}_{1p}^{(1)}\big) \end{bmatrix}, \tag{A3}$$

where the particular solutions $\hat{u}_{jp}^{(1)}$, $\hat{v}_{jp}^{(1)}$, $\hat{p}_{jp}^{(1)}$ and their gradients, given by (19), are taken at the interface $y = 0$, and only depend on the zeroth-order solution A_1, B_1, A_2, B_2 and c_0, and on the physical parameters.

The polynomials in the growth rate (21) for long waves are given by:

$$\begin{aligned} \mathrm{P}_0(m, d) = \frac{d^2}{60m^2 D_0^3}\big(&32d^9m^2 + m^2(56m + 135)d^8 + 4m^2\big(8m^2 + 61m + 49\big)d^7 \\ &+ 4m^2\big(34m^2 + 95m + 24\big)d^6 + 4m^3(57m + 49)d^5 + 2m^3\big(8m^2 + 57m - 4\big)d^4 \\ &+ 12m^4(m - 3)d^3 - 4m^4(2 + 5m)d^2 - 4m^5(m + 1)d - m^6\big), \end{aligned}$$

$$\mathrm{P}_1(m, d) = \frac{d^2}{60m^2 D_0^3}\big(d^{12} + (4m + 1)d^{11} + 4m(2m + 5)d^{10} + 12m(3m - 1)d^9$$

$$+ 2m\left(4m^2 - 57m - 8\right)d^8 - 4m^2(49m + 57)d^7 - 4m^2\left(24m^2 + 95m + 34\right)d^6$$
$$- 4m^2\left(49m^2 + 61m + 8\right)d^5 - m^3(135m + 56)d^4 - 32m^4d^3\big),$$

with

$$D_0 = d^4 + 4dm + 6d^2m + 4d^3m + m^2.$$

References

[1] Yih C.S., Instability due to viscous stratification, J. Fluid Mech. 27 (1967) 337–352.
[2] Hooper A.P., Long-wave instability at the interface between two viscous fluids: Thin layer effects, Phys. Fluids 28 (1985) 1613–1618.
[3] Hooper A.P., Boyd W.G.C., Shear-flow instability at the interface between two viscous fluids, J. Fluid Mech. 128 (1983) 507–528.
[4] Hinch E.J., A note on the mechanism of the instability at the interface between two shearing fluids, J. Fluid Mech. 144 (1984) 463–465.
[5] Charru F., Hinch E.J., "Phase diagram" of interfacial instabilites in two-layer Couette flow and mechanism for the long wave instability, J. Fluid Mech. (2000) (accepted for publication).
[6] Hooper A.P., The stability of two superposed viscous fluids in a channel, Phys. Fluids A 1 (1989) 1133–1142.
[7] Hooper A.P., Boyd W.G.C., Shear flow instability due to a wall and a viscosity difference at the interface, J. Fluid Mech. 179 (1987) 201–225.
[8] Renardy Y., Instability at the interface between two shearing fluids in a channel, Phys. Fluids 28 (1985) 3441–3443.
[9] Yiantsios S.G., Higgins B.G., Linear stability of plane Poiseuille flow of two superposed fluids, Phys. Fluids 31 (1988) 3225–3238.
[10] Barthelet P., Charru F., Fabre J., Experimental study of interfacial long waves in a two-layer shear flow, J. Fluid Mech. 303 (1995) 23–53.
[11] Sangalli M., Gallagher C.T., Leighton D.T., Chang H.-C., McCready M.J., Finite-amplitude waves at the interface between fluids with different viscosity: Theory and experiments, Phys. Rev. Lett. 75 (1995) 77–80.
[12] Charru F., Barthelet P., Secondary instabilities of interfacial waves due to coupling with a long wave mode in a two-layer Couette flow, Physica D 125 (1999) 311–324.
[13] Blennerhassett P.J., On the generation of waves by wind, Philos. T. Roy. Soc. A 298 (1980) 451–494.
[14] Hooper A.P., Grimshaw R., Nonlinear instability at the interface between two viscous fluids, Phys. Fluids 28 (1985) 37–45.
[15] Renardy Y., Weakly nonlinear behavior of periodic disturbances in two layer Couette–Poiseuille flow, Phys. Fluids A 1 (1989) 1666–1676.
[16] Renardy M., Renardy Y., Derivation of amplitude equations and analysis of sideband instabilities in two-layer flows, Phys. Fluids A 5 (1993) 2738–2762.
[17] Charru F., Fabre J., Long waves at the interface between two viscous fluids, Phys. Fluids 6 (1994) 1223–1235.
[18] Kao M.E.,, Park C., Experimental investigation of the stability of channel flows. Part 2. Two-layered co-current flow in a rectangular channel, J. Fluid Mech. 52 (1972) 401–423.
[19] Miles J.W., The hydrodynamic stability of a thin film of liquid in uniform shearing motion, J. Fluid Mech. 8 (1960) 593–610.
[20] Hanratty T.J., Interfacial instabilities caused by air flow over a thin liquid film, in Meyer R.E. (Ed.), Waves on Fluid Interfaces, Academic, New York, 1983, pp. 221–259.
[21] Miesen R., Boersma B.J., Hydrodynamic stability of a sheared liquid film, J. Fluid Mech. 301 (1995) 175–202.
[22] Timoshin S.N., Instabilities in a high-Reynolds-number boundary layer on a film-coated surface, J. Fluid Mech. 353 (1997) 163–195.
[23] Smith M.K., The axisymmetric long-wave instability of a concentric two-phase pipe flow, Phys. Fluids A 1 (1989) 494–506.
[24] Pozrikidis C., Instability of two-layer creeping flow in a channel with parallel-sided walls, J. Fluid Mech. 351 (1997) 139–165.
[25] Yih C.S., The mechanism for surface wave instability in film flow down an inclined plane, Phys. Fluids 6 (1963) 321–334.
[26] Chandrasekhar S., Hydrodynamic and Hydromagnetic Stability, Dover, New York, 1961.
[27] Yiantsios S.G., Higgins B.G., Rayleigh–Taylor instability in thin viscous films, Phys. Fluids A 1 (1989) 1484–1501.
[28] Orszag S.A., Accurate solution of the Orr–Sommerfeld stability equation, J. Fluid Mech. 50 (1971) 689–703.
[29] Albert F., Stabilité d'une interface entre deux fluides cisaillés: étude numérique et asymptotique, Thèse de Doctorat, Institut National Polytechnique de Toulouse, France, 1996.
[30] Drazin P.G., Reid W.H., Hydrodynamic Stability, Cambridge University Press, 1981.
[31] Kelly R.E., Goussis D.A., Lin S.P., Hsu F.K., The mechanism for surface wave instability in film flow down an inclined plane, Phys. Fluids A 1 (1989) 819–828.
[32] Goussis D.A., Kelly R.E., Mechanisms and conditions for an instability of shear flow in the presence of an interface, unpublished (1988).
[33] Boomkamp P.A.M., Miesen R.H.M., Classification of instabilities in parallel two-phase flow, Int. J. Multiphase Flow 22 (1996) 67–88.
[34] Joseph D.D., Renardy Y., Fundamentals of Two-fluid Dynamics. Vol. 1: Mathematical Theory and Applications, Springer-Verlag, 1993.